金属錯体における動的スピン平衡および連鎖する磁気物性の研究

小　島　憲　道*

*小島憲道　フェロー

Study on the Dynamical Spin Equilibrium and its Induced Successive Magnetic Phase Transition for Assembled Metal Complexes

Norimichi KOJIMA*

In general, the Fe^{III} site coordinated by six S atoms is in the low-spin (LS) state, while that coordinated by six O atoms is in the high-spin (HS) state. Therefore, it is expected that the spin state of Fe^{III} coordinated by three S atoms and three O atoms is situated in the spin-crossover region. From this viewpoint, in order to build an assembled metal complex system including $Fe^{III}O_3S_3$ site, we have synthesized $(C_6H_5)_4P[Zn^{II}Fe^{III}(mto)_3]$ (mto = C_2O_3S) consisting of $Fe^{III}O_3S_3$ and $Zn^{II}O_6$ octahedra and investigated the spin state of the $Fe^{III}O_3S_3$ site. The electron spin resonance (ESR) and ^{57}Fe Mössbauer spectra revealed that the rapid spin equilibrium in which the HS state and the LS state exchange in the time scale of $10^{-10} < \tau < 10^{-7}$ s occurs at the $Fe^{III}O_3S_3$ site. On the other hand, in the case of $(C_6H_5)_4P[Mn^{II}Fe^{III}(mto)_3]$ consisting of $Fe^{III}O_3S_3$ and $Mn^{II}O_6$, there exists a rapid spin equilibrium ($\tau < 10^{-7}$ s) between the HS and LS states at the $Fe^{III}O_3S_3$ site, which induces the frustration of internal magnetic field between the ferromagnetic and antiferromagnetic interactions on the $Mn^{II}O_6$ site. Owing to the frustration of internal magnetic field at the Mn^{II} site caused by the rapid spin equilibrium at the Fe^{III} site, $(C_6H_5)_4P[Mn^{II}Fe^{III}(mto)_3]$ undergoes the successive magnetic phase transitions at 30 K and 23 K.

1. INTRODUCTION

When a transition metal ion with an electron configuration of d^n ($n = 4-7$) is octahedrally coordinated by ligands, it is possible that the LS and HS states compete with each other in the ground state. If the ligand field splitting energy ($10Dq$) is smaller than the Coulomb interaction between electrons in the d orbitals, the electrons occupy the e_g (d_{x2-y2}, d_{z2}) and t_{2g} (d_{xy}, d_{yz}, d_{zx}) orbitals with the spin alignment determined by Hund's rule (HS state). On the other hand, if the ligand field splitting energy is large enough, Hund's rule is broken down because the Coulomb interaction energy between d electrons does not overcome $10Dq$, in which the spin configuration is called LS state. Therefore, the ground state of the transition metal ion with d^n ($n = 4-7$) configuration is determined by the competition between ligand field splitting and Coulomb interaction between d electrons. The energy diagram for d^n system called Tanabe-Sugano diagram is the most powerful method to analyze the competition between the HS and LS states as the ground state[1]. The Tanabe-Sugano diagram is a graph which plots the energy of multiplet terms against the ratio of ligand field (Dq) to the Racah parameter (B) representing the strength of Coulomb interaction. In the case of d^5 configuration, the Tanabe-Sugano diagram indicates that the ground state changes between HS ($Dq/B \leq 2.8$: $^6A_{1g}$) and LS ($Dq/B \geq 2.8$: $^2T_{2g}$) in the vicinity of $Dq/B = 2.8$. On the other hand, in the case of d^6 onfiguration, the Tanabe-Sugano diagram indicates that the ground state changes between HS ($Dq/B \leq 2.0$: $^5T_{2g}$) and LS ($Dq/B \geq 2.0$: $^1A_{1g}$) in the vicinity of $Dq/B = 2.0$. If the energy of ground state is close to HS and LS states, the system has a possibility to change the spin states between HS and LS by external perturbation, such as heat, applied pressure or light irradiation. Such the HS - LS transition is called spin-crossover phenomenon.

The spin-crossover phenomenon was observed for the first time by Cambi *et al*. in 1930s for tris(dithiocarbamato) iron(Ⅲ) complexes, $Fe^{III}(S_2CNR_2)_3$ (R = *n*-C_4H_9, *iso*-C_4H_9, etc.)[2]. They reported that the magnetic susceptibility changed remarkably depending on temperature caused by the gradual LS ($S = 1/2$) - HS ($S = 5/2$) transition. If the spin inter-conversion between LS ($S = 1/2$) and HS ($S = 5/2$) is slower than

2019年2月25日　受理
*豊田理化学研究所フェロー
東京大学名誉教授，理学博士
専門分野：分子集合体の物性化学，錯体化学，無機化学

the time scale ($\tau = 10^{-7}$ s) of ^{57}Fe Mössbauer spectroscopy, two kinds of quadrupole doublets corresponding to the HS and LS states are clearly distinguishable. On the other hand, if the spin inter-conversion is faster than 10^{-7} s, a single averaged quadrupole doublet is observed. In the case of $Fe^{III}(S_2CNR_2)_3$ (R = *n*-C_2H_5), the ^{57}Fe Mössbauer spectrum exhibits a broad quadrupole doublet in the temperature region of the gradual LS (S = 1/2) ↔ HS (S = 5/2) transition, which implies the rapid spin equilibrium between the HS and LS states is realized in the time scale of $\tau < 10^{-7}$ s[3]. Up to now, it has been reported that various kinds of spin-crossover Fe^{III} complexes consisting of $Fe^{III}S_6$, $Fe^{III}O_3S_3$, or $Fe^{III}N_4O_2$ octahedra exhibit the rapid spin equilibrium[4].

In general, the Fe^{III} site coordinated by six S atoms tends to be in the LS state, while the Fe site coordinated by six O atoms is in the HS state. Therefore, the spin state of $Fe^{III}O_3S_3$ would be situated in the spin-crossover region between the LS state of S = 1/2 and the HS state of S = 5/2. In fact, in the case of tris(monothio-β-diketonato) iron(Ⅲ) complexes, the LS (S = 1/2) and HS (S = 5/2) states coexist in the whole measuring temperature between 300 K and 80 K, and two kinds of doublet corresponding to the LS and HS states are clearly distinguished in the ^{57}Fe Mössbauer spectra, where the area of the LS state increases with decreasing temperature from 300 K to 80 K[5]. In the case of tris(monothiocarbamato) iron(Ⅲ) complexes, on the other hand, the rapid spin equilibrium occurs in which the HS and LS states exchange in the time scale of less than 10^{-7} s[6]. In this case, an averaged single doublet between the HS state (S = 5/2) and LS (S = 1/2) state is observed. In this way, it is expected that the spin state of Fe^{III} coordinated by three S atoms and three O atoms is situated in the spin-crossover region. However, the rapid spin equilibrium phenomenon has not yet been observed for assembled metal complex systems. From this viewpoint, in order to build an assembled metal complex system including $Fe^{III}O_3S_3$ site, we have synthesized $(C_6H_5)_4P[M^{II}Fe^{III}(mto)_3]$ (M = Mn, Zn; mto = C_2O_3S) consisting of $Fe^{III}O_3S_3$ and $M^{II}O_6$ octahedra and investigated the spin state of the $Fe^{III}O_3S_3$ site[7]. The spin states of the Fe^{III} sites for $Fe^{III}(ox)_3$ (ox = oxalato (C_2O_4)), $Fe^{III}(dto)_3$ (dto = dithiooxalato ($C_2O_2S_2$)), and $Fe^{III}(mto)_3$ are schematically shown in **Fig. 1**.

2. EXPERIMENTAL PROCEDURE

2.1 SYNTHESIS

[K_2(mto)]

K_2(mto) was prepared in the following way. Diethyl oxalate and KHS were dissolved in ethanol, then the solution was refluxed for 24 hours. After being evaporated, yellow colored precipitate was washed with ether and dissolved in ethanol. To this solution was added ethanol solution containing potassium hydroxide. After stirring, K_2(mto) was separated by suction filtration and washed with ether. The synthetic process of K_2(mto) is shown in **Scheme 1**.

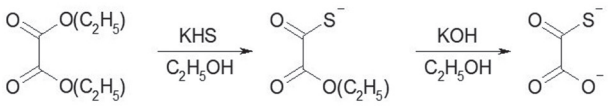

Scheme 1. Synthetic process of K_2(mto).

[$(C_6H_5)_4P[M^{II}Fe^{III}(mto)_3]$ (M = Zn, Mn)]

A methanol solution of $Fe^{III}(NO_3)_3 \cdot 9H_2O$ was added to a methanol solution of K_2(mto) and $(C_6H_5)_4PBr$. After stirring, $[Fe^{III}(mto)_3]^{3-}$ was obtained. This $[Fe^{III}(mto)_3]^{3-}$ solution was filtered to remove solid impurities. A methanol solution of $M^{II}Cl_2$ (M = Zn or Mn) was added to the filtrate. After being stirred, $(C_6H_5)_4P[M^{II}Fe^{III}(mto)_3]$ was obtained as red-brown colored powder by suction filtration and dried in vacuo.

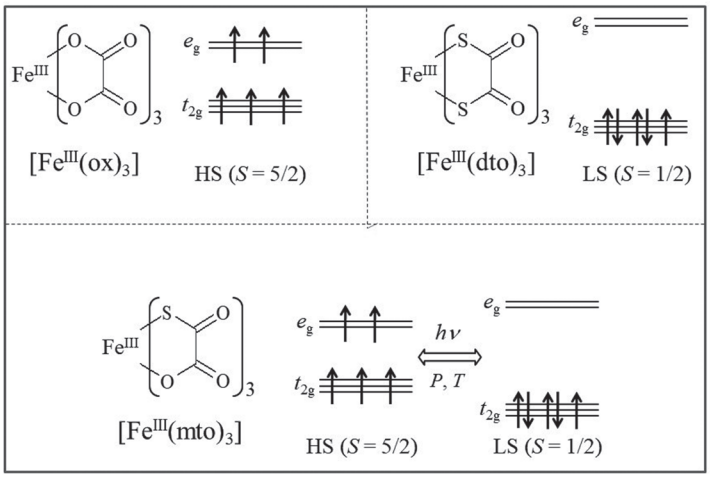

Figure 1. Spin states of the Fe^{III} sites for $Fe^{III}(ox)_3$, $Fe^{III}(dto)_3$, and $Fe^{III}(mto)_3$.

2.2 PHYSICAL MEASUREMENTS

Powder X-ray diffraction measurement was performed by a Rigaku multiflex at room temperature using a Cu K_α (λ = 1.54184 Å) radiation in the range of $2\theta = 3 - 60^\circ$ in order to determine the crystal parameters and space group.

The static magnetic susceptibility was measured by a Quantum Design, MPMS-5 SQUID susceptometer between 2 and 300 K under 0.5 T. The magnetic susceptibility data were corrected for the core diamagnetism estimated from Pascal's constant and the background of the polyethylene film. The zero-field cooled magnetization (ZFCM) and field-cooled magnetization (FCM) were also measured for investigating the ferrimagnetic phase of $(C_6H_5)_4P[Mn^{II}Fe^{III}(mto)_3]$ in the temperature range between 2 and 45 K under 3.0 mT. The remnant magnetization (RM) was measured in the same temperature region under zero field. The alternating-current (ac) magnetic susceptibility was measured between 2 and 40 K. The ac frequency was varied from 20 to 1000 Hz with amplitude of 0.3 mT.

The ESR measurement was performed between 10 and 300 K by a JEOL X-band (9.2 GHz) ESR spectrometer equipped with an Air Product LTR-3 cryostat.

For the ^{57}Fe Mössbauer spectroscopic measurements, ^{57}Co in Rh matrix was used as a Mössbauer γ-ray source. The spectra were calibrated by using the six lines of a body-centered cubic iron foil (α-Fe), the center of which was taken as zero isomer shift. An Iwatani Co. cryogenic refrigerator set, Cryomini and MiniStat was used with a temperature range from 10 to 300 K.

3. EXPERIMENTAL RESULTS and DISCUSSION

Figure 2 shows the powder X-ray diffraction pattern of $(C_6H_5)_4P[M^{II}Fe^{III}(mto)_3]$ (M = Mn, Zn), which resembles clearly that of $(n\text{-}C_3H_7)_4N[Fe^{II}Fe^{III}(dto)_3]$[8]. Based on the crystal structure of $(n\text{-}C_3H_7)_4N[Fe^{II}Fe^{III}(dto)_3]$ analyzed by the single crystal X-ray diffraction, the Rietveld analysis was performed for the powder X-ray diffraction pattern of $(C_6H_5)_4P[Mn^{II}Fe^{III}(mto)_3]$ at room temperature, which reveals the existence of a two-dimensional (2D) honeycomb network structure of $[Mn^{II}Fe^{III}(mto)_3]$ with intercalated counter cation of $(C_6H_5)_4P^+$. The lattice parameters are as follows; space group $P6_3$, $a = b$ = 9.79496(6) Å, c = 18.4812(15) Å, $\alpha = \beta = 90^\circ$, $\gamma = 120^\circ$, Z = 2. In this complex, the Mn^{II} and Fe^{III} atoms are alternately arrayed by the bridging ligand of mto, which forms the 2D honeycomb network structure of $[Mn^{II}Fe^{III}(mto)_3]$. The $(C_6H_5)_4P^+$ layer is intercalated between two adjacent $[Mn^{II}Fe^{III}(mto)_3]$ layers.

In $(n\text{-}C_4H_9)_4N[Zn^{II}Fe^{III}(ox)_3]$ with the similar structure of $(C_6H_5)_4P[Zn^{II}Fe^{III}(mto)_3]$, the χT value (= 4.22 cm^3 K mol^{-1}) is essentially constant in the whole temperature range of 4.2 – 300 K[9]. However, the χT value for $(C_6H_5)_4P[Zn^{II}Fe^{III}(mto)_3]$ decreases from 3.60 (at 300 K) to 2.66 cm^3 K mol^{-1} (at 4.2 K)[7]. In connection with this, it should be noted that the spin-only χT value is 4.375 cm^3 K mol^{-1} for the HS state (S = 5/2) of Fe^{III}, while that is 0.375 cm^3 K mol^{-1} for the LS state (S = 1/2) of Fe^{III}. Therefore, the χT value of $(C_6H_5)_4P[Zn^{II}Fe^{III}(mto)_3]$ is situated in the middle value between the magnetic moments for the HS and LS states of Fe^{III}.

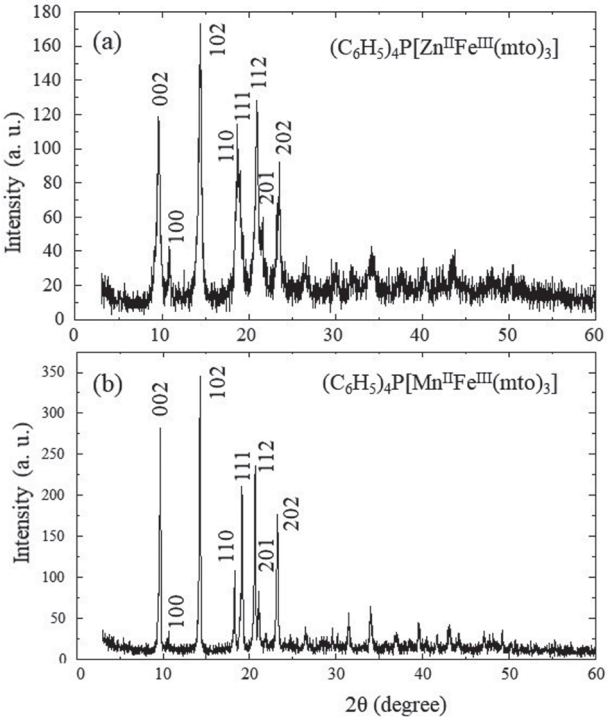

Figure 2. Powder X-ray diffraction pattern of $(C_6H_5)_4P[M^{II}Fe^{III}(mto)_3]$ (M = Mn, Zn)

Figure 3(a) shows the X-band ESR spectra for $(C_6H_5)_4P[Zn^{II}Fe^{III}(mto)_3]$ at 300, 77 and 10 K, in which the ESR signals corresponding to the HS state and the LS state of Fe^{III} site are clearly observed at around 300 mT ($g \approx 2.05$) and 150 mT ($g \approx 4.25$), respectively, in the temperature range between 300 and 10 K. The ESR signal ratio of the LS state to the HS state increases with decreasing temperature, which is consistent with the temperature dependence of $\chi_M T$. Therefore, these results indicate that the spin state of $Fe^{III}O_3S_3$ in $(C_6H_5)_4P[Zn^{II}Fe^{III}(mto)_3]$ is the spin equilibrium of the HS and LS states, where the HS and LS states are clearly distinguishable in the time scale (10^{-10} s) of X-band ESR spectroscopy. Figure 3(b) shows the ^{57}Fe Mössbauer spectra of $(C_6H_5)_4P[Zn^{II}Fe^{III}(mto)_3]$ at 300, 77 and 10 K. The single quadrupole doublet of Fe^{III} is observed despite of the coexistence of the HS and LS states in the ESR measurement between 300 and 10 K. Therefore, the ^{57}Fe Mössbauer spectra of $(C_6H_5)_4P[Zn^{II}Fe^{III}$

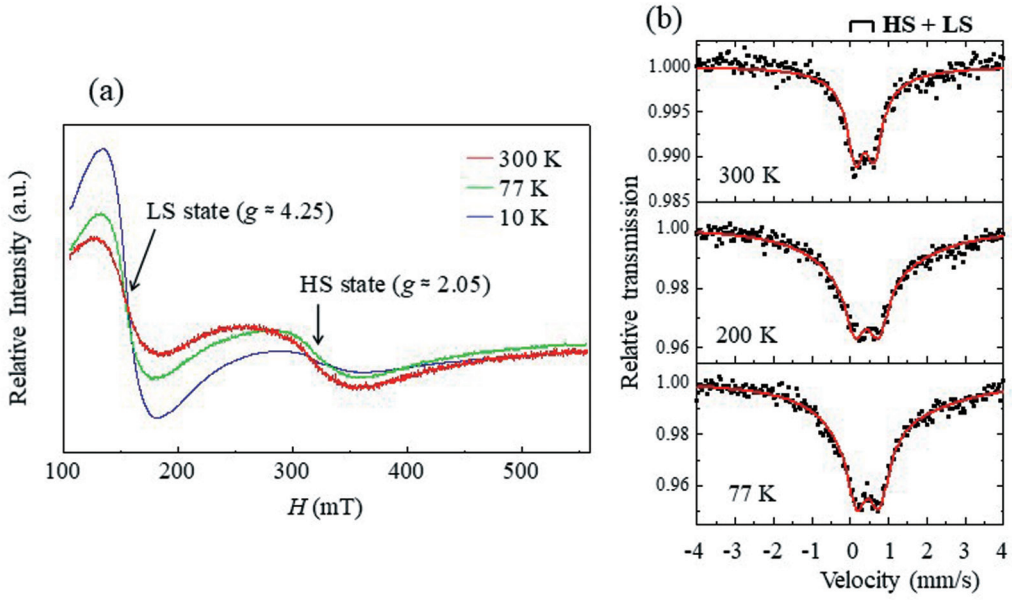

Figure 3. (**a**) X-band ESR spectra, and (**b**) ^{57}Fe Mössbauer spectra for $(C_6H_5)_4P[Zn^{II}Fe^{III}(mto)_3]$ at various temperatures[7].

$(mto)_3]$ indicates that the rapid spin equilibrium in which the HS and LS state exchange in the time scale faster than the time scale (10^{-7} s) of ^{57}Fe Mössbauer spectroscopy occurs at the $Fe^{III}O_3S_3$ site. The relaxation process between the HS and LS states at the $Fe^{III}O_3S_3$ site is considered to be a tunneling process. The time scale of spin equilibrium of Fe^{III} in $(C_6H_5)_4P[Zn^{II}Fe^{III}(mto)_3]$ is estimated at $10^{-10} < \tau < 10^{-7}$ s from the analysis of ESR and ^{57}Fe Mössbauer spectroscopy.

The tunneling probability for a non-radiative multi-phonon process from a given vibrational levels, m of the HS state and m' of the LS state, is given by the following equation[10],

$$W_{mm'} = \frac{2\pi}{\hbar^2\omega}\beta_{HL}^2 |<\chi_{m'}|\chi_m>|^2\ \delta(E_{m'}, E_m), \qquad (1)$$

where the electronic coupling matrix element $\beta_{HL} = <\psi_{LS}|H_{SO}|\psi_{HS}>$ is the second order spin-orbit coupling, $\hbar\omega$ is the energy of metal-ligand vibration, $\delta(E_{m'}, E_m)$ is the delta function ensuring energy conservation, $|<\chi_{m'}|\chi_m>|^2$ is the Franck-Condon factor of the overlap of the vibrational functions between the HS and LS states. At $T \approx 0$ K, since the vibrational ground state of the HS state is populated, the relaxation rate constant between the HS and LS states is expressed as follows[10],

$$k_{HL}(T \approx 0) = \frac{2\pi}{\hbar^2\omega}\beta_{HL}^2 |<\chi_n|\chi_0>|^2\ ,\ n = \frac{\Delta E_{HL}^0}{\hbar\omega}\ , \qquad (2)$$

where n is the zero-point energy difference expressed in units of vibrational quanta, and $|<\chi_n|\chi_0>|^2$ is expressed as follows,

$$|<\chi_n|\chi_0>|^2 = \frac{S^n e^{-S}}{n!}\ ,\ S = \frac{\frac{1}{2}f\Delta Q_{HL}^2}{\hbar\omega}\ , \qquad (3)$$

where S is the called Huang-Rhys factor[11], ΔQ_{HL} is the difference of horizontal displacement between the HS and LS potential wells in the metal-ligand coordinate geometry, f is the force constant. According to eq. (2) and eq. (3), with decreasing the Huang-Rhys factor, the Frank-Condon factor increases, which increases the relaxation rate constant between the HS and LS states. In general, the ΔQ_{HL} of spin crossover Fe^{III} complex is shorter than that of Fe^{II} complex. Indeed, the change in the Fe^{II}-ligand distance is 0.16 – 0.21 Å, while that in the Fe^{III}-ligand distance is about 0.12 Å[12].

From this viewpoint, we have focused on the spin crossover phenomena of $A[M^{II}Fe^{III}(mto)_3]$ (A = $(n\text{-}C_nH_{2n+1})_4N$, $(C_6H_5)_4P$, etc.; M = Mn, Fe, Zn, Cd). In the case of mto bridged hetero-metal complex system, $[Mn^{II}Fe^{III}(mto)_3]$ consisting of $Mn^{II}O_6$ and $Fe^{III}O_3S_3$ octahedra, the spin states of the Mn^{II} and Fe^{III} sites are considered to be the HS state and the spin equilibrium state of HS ↔ LS, respectively. If the spin state of Fe^{III} site is LS (S = 1/2) state, there exist four potential exchange interactions (J_P) and one kinetic exchange interaction (J_K) between the Fe^{III} and Mn^{II} sites. The sum of the potential exchange interaction is consideroed to be stronger than the kinetic exchange interaction, which is responsible for the ferromagnetic ordering. In connection with this, the following should be mentioned. The ferromagnetic ordering of $(n\text{-}C_3H_7)_4N[Mn^{II}Fe^{III}(dto)_3]$ with Mn^{II} (S = 5/2) and Fe^{III} (S = 1/2) has been reported[13], in which the Curie temperature (T_C) and the Weiss temperature (θ) were estimated at 4 K and 10

K, respectively, from the analysis of magnetization and magnetic susceptibility as a function of temperature. On the other hand, if the spin state of Fe^{III} site is the HS (S = 5/2) state, there exist five kinetic exchange interactions (J_K) between the Fe^{III} and Mn^{II} sites, which is considered to be stronger than the potential exchange interactions between the Fe^{III} and Mn^{II} sites, which is responsible for the ferrimagnetic ordering. Indeed, the ferrimagnetic ordering of $(n\text{-}C_nH_{2n+1})_4N[Mn^{II}Fe^{III}(ox)_3]$ with Mn^{II} (S = 5/2) and Fe^{III} (S = 5/2) has been reported[14], in which T_N was estimated at 27 – 28 K.

Therefore, if the spin state of the Fe^{III} site in the $[Mn^{II}Fe^{III}(mto)_3]$ system behaves as the dynamical spin equilibrium phenomenon, the internal magnetic field at the Mn^{II} site should be frustrated between the ferromagnetic and antiferromagnetic interactions with a rapid time scale around 10^{-7} s, which is schematically shown in **Fig. 4**.

Based on this viewpoint, we have synthesized $(C_6H_5)_4P[Mn^{II}Fe^{III}(mto)_3]$ and investigated the magnetic properties[15]. The molar magnetic susceptibility (χ_M) as a function of temperature has a broad maximum, typical character of 2D Heisenberg-type antiferromagnet, at around 50 K, and shows a steep increase below 30 K with a hump at around 23 K, where both of the real (χ') and imaginary (χ'') parts in ac magnetic susceptibility exhibit steep peaks indicating a magnetic phase transition, which is shown in **Fig. 5**(b). As shown in Fig. 5(a), the field cooled magnetization shows a rapid increase below 30 K, and almost saturates below 23 K. At 30 K, the remnant magnetization and the magnetic hysteresis loop disappear. Therefore, it is obvious that $(C_6H_5)_4P[Mn^{II}Fe^{III}(mto)_3]$ undergoes two successive magnetic phase transitions at 30 K and 23 K. The ^{57}Fe Mössbauer spectroscopy for $(C_6H_5)_4P[Mn^{II}Fe^{III}(mto)_3]$ implies that the spin state at the Fe^{III} site is still para-magnetic even at 24 K. At 23 K, both of the Mn^{II} and Fe^{III} spins are eventually ordered. It is considered that the successive magnetic phase transitions in $(C_6H_5)_4P[Mn^{II}Fe^{III}(mto)_3]$ are induced by the rapid spin equilibrium at the Fe^{III} site.

Taking account of the temperature dependences of the magnetization, ac magnetic susceptibility, and ^{57}Fe Mössbauer spectra for $(C_6H_5)_4P[Mn^{II}Fe^{III}(mto)_3]$, the Gibbs energies of the A, B and C phases as a function of temperature for $(C_6H_5)_4P[Mn^{II}Fe^{III}(mto)_3]$ are schematically represented in **Fig. 7**, in which the A, B and C phases are defined as follows,

Phase A: The spins at the Mn^{II} and Fe^{III} sites are paramagnetic.

Phase B: The spin at the Mn^{II} site is ordered, while that at the Fe^{III} site is still paramagnetic.

Phase C: Both of the spins at the Mn^{II} and Fe^{III} sites are ordered.

As shown in Fig. 7, with decreasing temperature, the first magnetic phase transition from phase A to phase B takes place at 30 K, then the second magnetic phase transition from phase B to phase C takes place at 23 K.

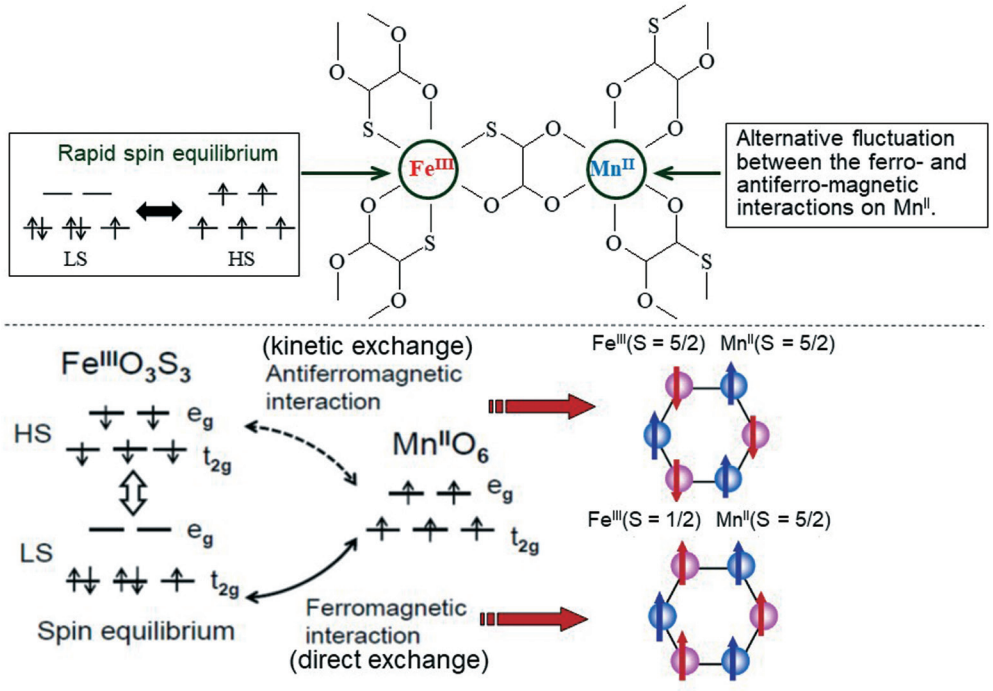

Figure 4. Relationship between the rapid spin equilibrium of the Fe^{III} site and the dynamical frustration of internal magnetic field at the Mn^{II} site in the $[Mn^{II}Fe^{III}(mto)_3]$ system.

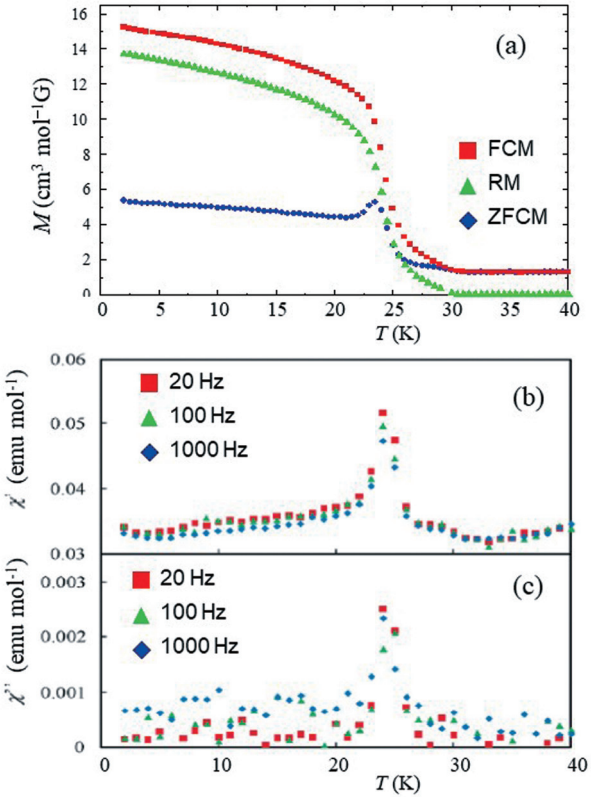

Figure 5. (**a**) Magnetization, (**b**) in-phase ac magnetic susceptibility, (**c**) out-phase ac magnetic susceptibility of $(C_6H_5)_4P[Mn^{II}Fe^{III}(mto)_3]$ as a function of temperature. The temperature dependence of the zero-field-cooled magnetization (ZFCM) and the field-cooled magnetization (FCM) were measured in the temperature range of 40 – 2 K under 3.0 mT. The remnant magnetization (RM) was measured in the same temperature range under zero field. The ac magnetic susceptibility measurements were performed in the temperature range of 40 – 2 K under ac magnetic field of 0.3 mT and frequency range of 20 – 1000 Hz.

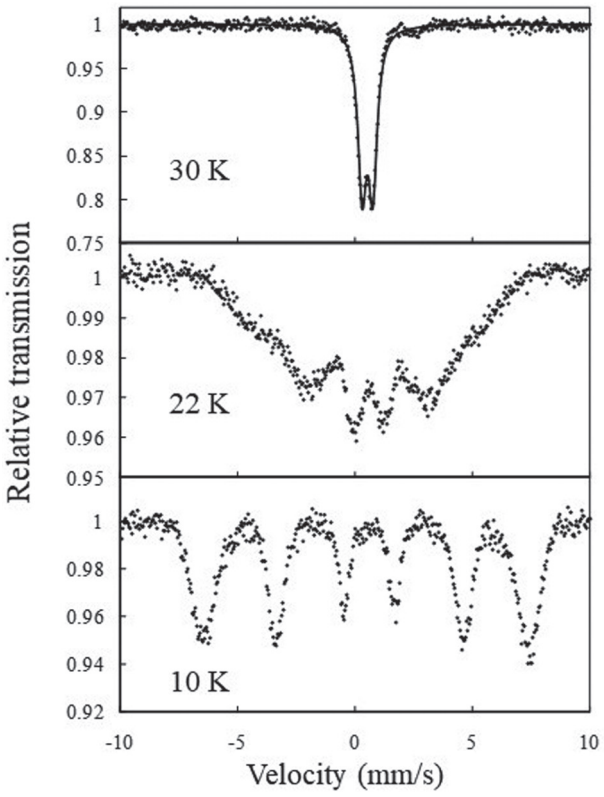

Figure 6. ^{57}Fe Mössbauer spectra of $(C_6H_5)_4P[Mn^{II}Fe^{III}(mto)_3]$ between 30 K and 10 K.

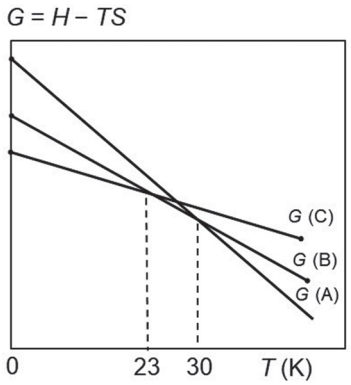

Figure 7. Schematic Gibbs energies of the A, B and C phases as a function of temperature for $C_6H_5)_4P[Mn^{II}Fe^{III}(mto)_3]$. G(A), G(B) and G(C) show the Gibbs energies for the A, B and C phases, respectively. Phase A: The spins at the Mn^{II} and Fe^{III} sites are paramagnetic, Phase B: The spin at the Mn^{II} site is ordered, while that at the Fe^{III} site is still paramagnetic, Phase C: Both of the spins at the Mn^{II} and Fe^{III} sites are ordered.

4. CONCLUSION

In general, the Fe^{III} site coordinated by six S atoms is in the low-spin (LS) state, while that coordinated by six O atoms is in the high-spin (HS) state. Therefore, it is expected that the spin state of Fe^{III} coordinated by three S atoms and three O atoms is situated in the spin-crossover region. From this viewpoint, in order to build an assembled metal complex system including $Fe^{III}O_3S_3$ site, we have synthesized $(C_6H_5)_4P[Zn^{II}Fe^{III}(mto)_3]$ consisting of $Fe^{III}O_3S_3$ and $Zn^{II}O_6$ octahedra and investigated the spin state of the $Fe^{III}O_3S_3$ site. The electron spin resonance (ESR) and ^{57}Fe Mössbauer spectra revealed that the rapid spin equilibrium in which the HS state and the LS state exchange in the time scale of $10^{-10} < \tau < 10^{-7}$ s occurs at the $Fe^{III}O_3S_3$ site. On the other hand, in the case of $(C_6H_5)_4P[Mn^{II}Fe^{III}(mto)_3]$ consisting of $Fe^{III}O_3S_3$ and $Mn^{II}O_6$, there exists a rapid spin equilibrium ($\tau < 10^{-7}$ s) between the HS and LS states at the $Fe^{III}O_3S_3$ site, which induces the frustration of internal magnetic field between the ferromagnetic and antiferromagnetic interactions at the $Mn^{II}O_6$ site. Owing to the frustration of internal magnetic field at the Mn^{II} site caused by the rapid spin equilibrium at the Fe^{III} site, $(C_6H_5)_4P[Mn^{II}Fe^{III}(mto)_3]$ undergoes the successive magnetic phase transitions at 30 K and 23 K. At 30 K, the first magnetic phase transition from phase A to phase B takes place. Above

30 K, the spins at the Mn^{II} and Fe^{III} sites are paramagnetic. Below 30 K, on the other hand, the spin at the Mn^{II} site is ordered, while that at the Fe^{III} site is still paramagnetic. At 23 K, the second magnetic phase transition from phase B to phase C takes place, in which both of the spins at the Mn^{II} and Fe^{III} sites are ordered.

ACKNOWLEDGMENT

The author wishes to thank Prof. M. Enomoto (Tokyo University of Science), Dr. A. Okazawa (The University of Tokyo), Dr. K. Kagesawa (Tohoku University) and Dr. Y. Ono (Mitsubishi Chemical Co.) for the fruitful collaboration and Mr. H. Hasegawa (WDB) for the support of synthesizing various materials. This work has been supported by Toyota Physical and Chemical Research Institute, and a Grant-in-Aid for Science Research from the Ministry of Education, Science, Sports and Culture.

REFERENCES

1) Y. Tanabe and S. Sugano, *J. Phys. Soc. Jpn*., **9** (1954) 766.
2) ***a)*** L. Cambi and A. Cagnasso, *Atti Accad. Naz. Lincei*., **13** (1931) 809, ***b)*** L. Cambi, L. Szegö and A. Cagnasso, *Atti Accad. Naz. Lincei*., **15** (1932) 266, ***c)*** L. Cambi and L. Szegö, *Ber. Deutsch. Chem. Ges*., **66** (1933) 656.
3) J. M. Fiddy, I. Hall, F. Gradjean, U. Russo and G. J. Long, *Inorg. Chem*., **26** (1987) 4138.
4) ***a)*** K. R. Kunze, D. L. Perry and L. J. Wilson, *Inorg. Chem*., **16** (1977) 594, ***b)*** H. Oshio, Y. Maeda and Y. Takahashi, *Inorg. Chem*., **22** (1983) 2684, ***c)*** Y. Maeda, N. Tsutsumi and Y. Takahashi, *Inorg. Chem*., **23** (1984) 2440, ***d)*** M. D. Timken, A. M. Abdel-Mawgoud and D. N. Hendrickson, *Inorg. Chem*., **25** (1985) 160, ***e)*** M. Nihei, T. Shiga, Y. Maeda and H. Oshio, *Coord. Chem. Rev*., **251** (2007) 2606.
5) M. Cox, J. Darken, B. W. Fitzsimmons, A. W. Smith, L. F. Larkworthy and K. A. Rogers, *J. Chem. Soc. Dalton Trans*., (1972) 1192.
6) K. R. Kunze, D. L. Perry and L. J. Wilson, *Inorg. Chem*., **16** (1977) 594.
7) ***a)*** K. Kagesawa, A. Okazawa, M. Enomoto and N. Kojima, *Chem. Lett*., **39** (2010) 872, ***b)*** K. Kagesawa, *Doctoral Thesis*, (The University of Tokyo, 2011).
8) M. Itoi, A. Taira, M. Enomoto, N. Matsushita, N. Kojima, Y. Kobayashi, K. Asai, K. Koyama, T. Nakamoto, Y. Uwatoko and J. Yamamura, *Solid State Commun.,* **130** (2004) 415.
9) H. Ōkawa, N. Matsumoto, H. Tamaki and M. Ohba, *Mol. Cryst. Liq. Cryst*., **233** (1993) 257.
10) A. Hauser, in *Spin Crossover in Transition Metal Compounds II*, P. Gütlich, H. A. Goodwin (Eds.), Springer-Verlag, 2004, pp. 155-198.
11) T. C. Brunold and H. U. Güdel, in *Inorganic Electronic Structure and Spectroscopy I*, E. I. Solomon, A. B. P. Lever (Eds.), Wiley, 1999, p. 259.
12) ***a)*** J.-F. Létard, G. Chastanet, P. Guionneau and C. Desplanches, in *Spin-Crossover Materials: Properties and Applications.* M. A. Halcrow (Ed.), Wiley, 2013, pp. 475-506, ***b)*** Y. Moritomo, K. Kato, A. Nakamoto, N. Kojima, E. Nishibori, M. Takata and M. Sakata, *J. Phys. Soc. Jpn*., **71** (2002) 1015.
13) ***a)*** S. G. Carling, J. M. Bradley, D. Visser and P. Day, *Polyhedron,* **22** (2003) 2317, ***b)*** M. Enomoto, H. Ida, A. Okazawa and N. Kojima, *Crystals*, **8** (2018) 446.
14) C. Mathonière, C. J. Nuttall, S. G. Carling and P. Day, *Inorg. Chem*., **35** (1996) 1201.
15) N. Kojima and A. Okazawa, in *Modern Mössbauer Spectroscopy: New Challenges Based on Cutting-Edge Techniques*, Y. Yoshida, G. Langouche (Eds.), Springer-Nature, 2019, Ch. 6.